applied sciences

MDPI

Article

Optimization of Structural Parameters of Venturi Vertical Cooling Furnace

Haifeng Li [1,2,*], Tengfei Qi [2] and Yongjie Zhang [2]

1 Key Laboratory for Ecological Metallurgy of Multimetallic Mineral (Ministry of Education), Northeastern University, Shenyang 110819, China
2 School of Metallurgy, Northeastern University, Shenyang 110819, China; muller1970@163.com (T.Q.); zyj@baosteel.com (Y.Z.)
* Correspondence: lihf@smm.neu.edu.cn

Abstract: Theoretically, the vertical sinter sensible heat recovery process can significantly improve the recovery rate of sinter sensible heat. However, the segregated distribution of the sinter and uneven gas–solid flow in vertical cooling furnaces result in insufficient contact and heat exchange between the high-temperature sinter and the cooling gas, thereby limiting the improvement in the sinter sensible heat recovery rate. A Venturi vertical cooling furnace can improve the contact heat transfer between gases and solids and the uniformity of the sinter and the cooling gas temperature. However, this leads to a significant increase in the gas pressure drop and affects the integrity of the downward movement of the sinter. To control the increase in the gas pressure drop while increasing the sensible heat recovery and maintaining the integral flow of the sinter, this study takes a Meishan Steel vertical cooling furnace as the research object and uses the DEM-CFD coupling model to optimize the structural parameters of the Venturi-type vertical cooling furnace. Firstly, a scaling method was designed to reduce the computational cost. Secondly, based on the on-site conditions, the selection range of structural parameters for the Venturi furnace was determined. Finally, an orthogonal experiment was designed. Taking the sensible heat recovery of the sinter and the pressure drop of the cooling gas as the main index, the integrity of the sinter flow was taken as the secondary index to study the Venturi structure parameters suitable for the Meishan Steel vertical cooling furnace, including the width of the vertical part w, the length of the vertical part l, the contraction angle of the contraction part β, and the expansion angle of the expansion part α. The results showed that the order of structural parameters affecting the sensible heat recovery was w, β, α, and l, and the order of parameters affecting the gas pressure drop was w, β, l, and α. The appropriate structural parameters of the Venturi furnace type, obtained by considering the sensible heat recovery and gas pressure drop, were w = 1.1 m, β = 16°, α = 13°, and l = 0.5 m. In addition, in order to improve the integrity of the sinter flow, it was also necessary to increase the wall friction of the particles in the central area of the vertical section by adding steel plates. The results can provide theoretical guidance for improvements to the Meishan Steel vertical cooling furnace. The operation parameters corresponding to the Venturi furnace type can be studied later.

Keywords: sinter; vertical cooling furnace; Venturi furnace type; gas–solid heat transfer; orthogonal experiments

check for updates

Citation: Li, H.; Qi, T.; Zhang, Y. Optimization of Structural Parameters of Venturi Vertical Cooling Furnace. *Appl. Sci.* **2023**, *13*, 12858. https://doi.org/10.3390/app132312858

Academic Editors: Branislav Bul'ko, Mária Hagarová and Dana Baricová

Received: 6 November 2023
Revised: 25 November 2023
Accepted: 27 November 2023
Published: 30 November 2023

1. Introduction

The energy consumption of the sintering process in China accounts for about 15% of the entire iron and steel industry, second only to the ironmaking process. The recovery of sintering waste heat is an important means to reduce the energy consumption and improve the energy efficiency in the sintering process. At present, the recovery rate of sintering waste heat in China is low, only about 40% [1]. Sintering waste heat mainly includes two parts: sintering flue gas waste heat and sintering ore sensible heat, accounting for about 27% and 45% [2] of the total sintering heat expenditure, respectively. Compared to the waste heat from sintering flue gas, the amount of sensible heat in sintering ore is large, the quality is high, and it is easily carried by air, making it a key focus for the recovery of the waste heat resources from sintering. At present, the sensible heat recovery of sinter is mainly carried out in a ring cooler. Statistics show that only 42% of the sensible heat of sinter can be recovered. As much as 32% of the waste heat of medium- and low-temperature flue gas is released directly. The ring-cooling process inevitably has some disadvantages, such as a large amount of air leakage and the unorganized discharge of dust. Based on this, and inspired by coke dry quenching (CDQ) technology [3], relevant scholars put forward the sinter sensible heat vertical recovery process [4], which changes the heat transfer mode, transforming gas–solid cross-flow horizontal ring cooling into vertical gas–solid countercurrent vertical cooling. Theoretically, the outlet gas temperature can be maintained at a higher level of 400~500 °C. This is expected to increase the sensible heat recovery from 40% to 80%. A vertical cooling furnace is the core piece of equipment of the sinter sensible heat vertical recovery process, and its furnace structure has an important influence on the countercurrent heat transfer between the high-temperature sinter and the cooling gas in the furnace. Therefore, it is necessary to study the structure of vertical cooling furnaces and the range of reasonable parameters.

Due to the sinter sensible heat vertical recovery process being put forward with reference to CDQ technology, the design of a vertical cooling furnace often refers to a type of dry quenching furnace. The appropriate parameters have been studied by relevant scholars. Xu [5] established a two-dimensional steady-state model based on porous media theory and the local thermal non-equilibrium model and, with the goal of minimum loss, used the multi-objective genetic algorithm of a backpropagation (BP) neural network to propose a suitable height–diameter ratio and gas–solid ratio for a given size of a vertical cooling furnace. Taking the maximum enthalpy exergy of the outlet cooling gas as the target, Feng [6,7] optimized the inner diameter and height of a vertical cooling furnace, the inlet cooling gas temperature, the flow rate, and the particle size of the sinter and put forward the appropriate values of the corresponding parameters for a vertical cooling furnace matched with a 360 m^2 sintering machine. Taking the exergy value and exergy efficiency of hot gas as indices, Fu [8] obtained suitable parameters such as the height–diameter ratio, the volume, and the temperature of the cooling gas, which formed a suitable model for a vertical cooling furnace. Chen [9] studied the effects of the gas–solid ratio, the cooling height, and the diameter on the gas–solid heat transfer in a vertical cooling furnace with the target of hot flue gas exergy and obtained the appropriate structure and process parameters of the studied object. Zhang [10] took into account the effects of the inner diameter and the height of the vertical cooling furnace and the mass flow rate of the sinter and the cooling air on the enthalpy of the outlet cooling air, the fan energy consumption, and the dimensionless exergy loss and obtained the appropriate structure and process parameters. Xu [11] found the structure and operating parameters of a waste-heat-recovery vertical tank corresponding to a sintering machine with an annual output of 2.6 million tons through an analytical calculation, using the values of hot flue gas exergy and gas resistance loss as evaluation indicators.

The above studies were often based on the porous media model; they assumed that the particle size and voidage distribution of the sinter bed were uniform and regarded the sinter bed as static or uniformly moving down in the vertical direction. However, in the actual production process, the particle size and voidage distribution in vertical cooling furnaces are not uniform due to distribution segregation, and it is difficult to realize the overall downward movement of sinter. This makes the above hypotheses different from the actual situation. The operational result [12,13] of a Meishan Steel vertical cooling furnace also shows that the boundary effect is serious due to the segregation of sinter distribution in the vertical cooling furnace. The sinter in the sidewall area is cooled transiently due to a greater quantity of cooling gas, while the sinter in the central area is not cooled due to a lower quantity of cooling gas, resulting in the uneven cooling of the sinter, which seriously affects the improvement of the sensible heat recovery rate of the sinter.

Based on this, the authors' team proposed a Venturi furnace type [14] from the perspective of optimizing the shape of the vertical cooling furnace cavity and found that this furnace type can improve the gas–solid contact characteristics, strengthen the gas–solid convective heat transfer, and improve the uniformity of the temperature distribution of sinter and cooling air along the width direction at the cost of increasing the pressure drop of cooling gas. Further research has been conducted on the improvement effect of this furnace type on the distribution of sinter and the gas–solid flow inside the furnace [15]. It has been found that this furnace type can increase the porosity of the sinter bed in the middle zone of the furnace cavity, maintain the integrity of the sinter flow, and improve the uniformity of the cooling airflow distribution. In order to further increase the heat transfer between gases and solids while controlling the increase in the gas pressure drop, this study takes the Meishan Steel vertical cooling furnace as the research object based on the team's previous research. Firstly, combined with the site conditions, the structural parameters and value range of the Venturi furnace were determined. Then, the orthogonal experiment was designed according to the relevant factors and levels. Finally, taking the sensible heat recovery of the sinter and the pressure drop of the cooling gas as the main index and the integrity of sinter flow as the secondary index, the structural parameters of the Venturi furnace suitable for the Meishan Steel vertical cooling furnace were studied in order to provide a theoretical basis and design scheme for optimizing the Meishan Steel vertical cooling furnace.

2. Mathematical and Physical Model

Considering the influence of the furnace structure on sinter particle accumulation, a discrete element method (DEM)–computational fluid dynamics (CFD) coupled model was used to describe the gas–solid heat transfer behavior. The motion and heat transfer between particles were solved using the Hertz–Medellin (no-slip) model and the heat conduction model under the Lagrangian framework [16]. The flow and heat transfer of the fluid phase between the particle phases were calculated using the continuity equation, the Navier–Stokes equation, and the energy conservation equation based on local average variables. The drag force was considered the main force between the particle phase and the fluid phase. In this study, Ergun's and Wen and Yu's drag model [17] was used to describe the drag force on particles. The convective heat transfer between the particle phase and the fluid phase is described by the Ranz–Marshall model, and the accuracy of this model for the calculation of gas–solid heat transfer has been verified [18–20]. The specific expression in the above model is detailed in Refs. [14,15]. Ref. [21] indicated that the cooling gas in the vertical cooling furnace exhibited turbulent flow. The standard k–ε turbulence model is widely used in engineering calculations, and this algorithm has the characteristics of high computational accuracy, simplicity, and stability. Therefore, this study also used the standard k–ε turbulence model to calculate the turbulent flow of gas in the vertical cooling furnace. The commercial software EDEM 2020 and ANSYS Fluent 2020 were used for the simulation calculation.

The Meishan Steel vertical cooling furnace is composed of six bins, and its overall and single-bin structures are shown in Figure 1a,b. In this study, the cuboid furnace cavity was transformed into a Venturi furnace cavity. First, a contraction structure was added at the lower part of the original furnace cavity. Then, the center vent cowl was raised to correspond to the contraction structure of the side wall to form an expansion structure. The existence of the contraction structure and expansion structure made the channel width of the furnace cavity change in space, forming a contraction–vertical–expansion Venturi structure, as shown in Figure 1c. At this time, the Venturi furnace type involves four structural parameters: the width w and length l of the vertical part, the contraction angle of the contraction part β, and the expansion angle of the expansion part α, as shown in Figure 1d. In order to improve the calculation efficiency, the buffer bin, distribution pipe, crisscross beam, and other structures were ignored. At the same time, a slice was cut from the center of the furnace cavity, and half of the region was selected as the calculation domain. The thickness of the slice was 5 times the maximum particle size (750 mm) to eliminate the effect of front- and rear-wall friction on particle motion, as shown in Figure 1e.

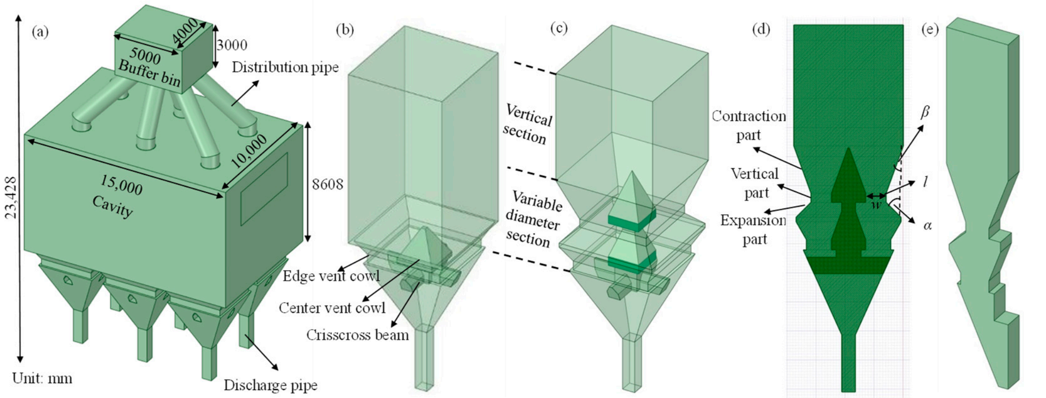

Figure 1. Existing furnace type and Venturi furnace type. (**a**) Existing furnace type; (**b**) single bin; (**c**) Venturi furnace type; (**d**) structure parameters of Venturi furnace; (**e**) slot model.

3. Simulation Conditions

3.1. Physical Parameters

The selected sinter particles were from the No. 3 Meishan Steel sintering machine, with a wide particle size distribution of 0~150 mm. In order to retain this feature and take into account the calculation cost, the lower limit of sinter feeding size was raised to 10 mm. For particles with a particle size of less than 10 mm, the mass fraction was incorporated into the 10~25 mm particle size range. The mass fraction of each particle size section was determined according to the actual production situation of the Meishan Steel vertical cooling furnace, and the sinter particle size in the section was randomly generated. The detailed particle size distribution is shown in Table 1.

Table 1. Sinter particle size distribution and mass fraction.

Particle Size (mm)	10~25	25~40	40~80	80~150
Mass fraction (%)	20	35	30	15

The bulk density and packing angle are the comprehensive embodiment of the particle property parameters, which play a key role in the accuracy of the discrete element simulation results. In this study, the bulk density calibration and stacking angle calibration were carried out according to the method in Ref. [22]. The simulation parameters obtained from the calibration are shown in Table 2.

Table 2. Simulation parameters.

Parameters	Poisson's Ratio	Density ($kg \cdot m^{-3}$)	Shear Modulus (MPa)	Restitution Coefficient	Coefficient of Sliding Friction	Coefficient of Rolling Friction
Sinter	0.25	2.6×10^3	3.5×10^1	–	–	–
Wall	0.30	7.8×10^3	7.0×10^4	–	–	–
Sinter–sinter	–	–	–	0.25	0.38	0.08
Sinter–wall	–	–	–	0.20	0.45	0.16

3.2. Model Scaling

Under the above simulation conditions, the number of particles accumulated in the slot model reached 3.66×10^4. The efficiency of the DEM–CFD coupling calculation was low due to the large number of particles. Therefore, the method of scaling the physical model was proposed to further improve the computational efficiency. Firstly, the different structural parameters of the Venturi furnace resulted in different height–diameter ratios. And different height–diameter ratios often correspond to different optimal gas–solid ratios. Therefore, under the same gas-to-solid ratio, it may be the case that this gas-to-solid ratio had a better heat transfer effect for one type of Venturi structure, but a worse effect for another, resulting in a comparison between better and worse heat transfer effects. Considering the large adjustable range of the sinter capacity and the cold air flow rate in the Meishan Steel vertical cooling furnace, in order to eliminate the influence of the gas–solid heat transfer caused by the gas–solid ratio, the fixed-bed heat transfer mode was proposed in this study. At this time, the particles did not move except for the accumulation process. Therefore, the thickness of the slot model was reduced to 3 times [23] the maximum particle size (450 mm). Secondly, the physical model was reduced by introducing a scaling factor. Only the upper limit of particle size was reduced, and the rest of the particle size and the mass fraction were kept unchanged. Thus, the number of particles was reduced while the characteristics of a wide particle size distribution were maintained. Thirdly, the physical model and the upper limit of particle size used the same scaling factor, so the width–diameter ratio of the slot model remained unchanged. See Table 3 for detailed scaling.

Table 3. Model scaling settings.

Scaling Factor	Width (mm)	Width–Diameter Ratio	Upper Limit of Particle Size (mm)	Particle Diameter Ratio	Particle Number	Voidage	Average Diameter(mm)
1.0	2400	16	150	15:1	366,060	0.395	22.39
0.8	1920	16	120	12:1	181,663	0.415	22.43
0.7	1380	16	105	10.5:1	121,893	0.418	22.50
0.6	1440	16	90	9:1	75,929	0.423	22.56

It can be seen from Table 3 that with the above scaling method, the particle size ratio was still basically maintained at about 10:1; that is, the particles were still basically widely distributed. Therefore, the scaled sinter packed bed could still simulate the filling effect of relatively small particles in the large particle gap. The number of sinter particles decreased significantly, which improved the calculation efficiency. The maximum variation range of the average voidage was only 7%, while the average particle size hardly changed.

The gas velocity distribution in the furnace after scaling was further studied to determine the appropriate scaling factor. In this study, the particles were densely packed and moved down slowly, and the particle size used in the reduction model was close to that of the actual furnace. Therefore, the Reynolds number [24] was selected to determine the inlet gas velocity of the scaled model.

According to the equality of the Reynolds numbers between the prototype and the model, the inlet velocity of the scaled model was calculated to obtain the gas velocity distribution inside the vertical cooling furnace under different scaling conditions, as shown in Figure 2. It can be seen that after the calculation domain was reduced, the gas velocity distribution cloud map was similar. To quantitatively compare the distribution of the gas velocity along the transverse direction, the ratio of the gas velocity at each point on different height planes L1~L4 to the average gas velocity on the plane was extracted as a dimensionless velocity, and the distribution of dimensionless velocity on L1~L4 was plotted, as shown in Figure 3. On plane L3, the gas velocity curves corresponding to three scaling factors were very similar to the prototype. On plane L2, the dimensionless velocity corresponding to the scaling factor of 0.6 was generally higher, and the velocity curve was also significantly different from the prototype. On planes L1 and L4, the velocity curve corresponding to the scaling factor of 0.7 was even closer to the prototype.

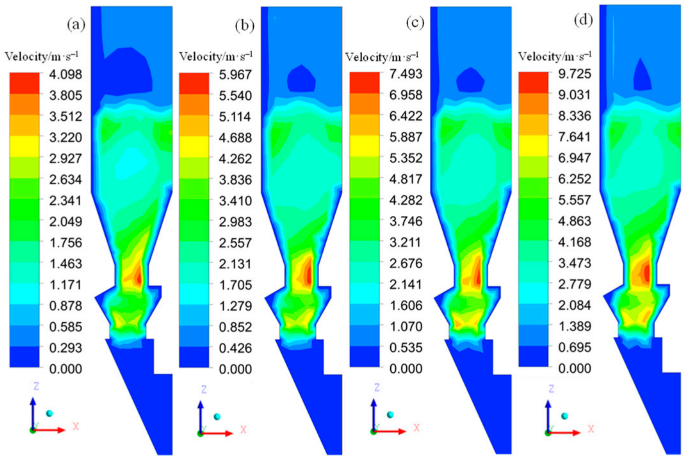

Figure 2. Gas velocity distribution under different scaling factors: (**a**) 1.0; (**b**) 0.8; (**c**) 0.7; (**d**) 0.6.

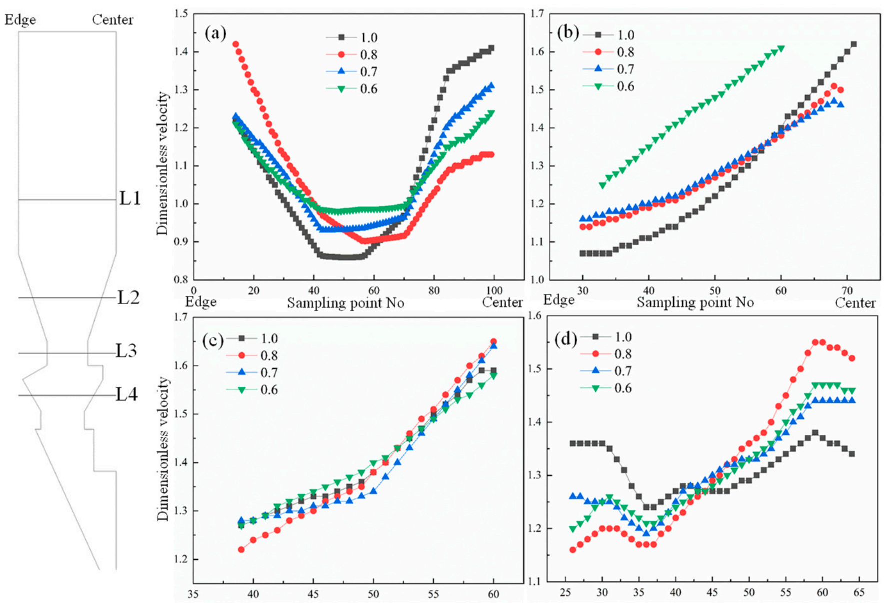

Figure 3. Gas velocity distributions on L1~L4. (**a**) L1; (**b**) L2; (**c**) L3; (**d**) L4.

Combined with the comparative results of the particle number, voidage, and gas velocity distribution, it was necessary to take into consideration both the simulation accuracy and the calculation cost; the scaling factor was determined to be 0.7. In addition, from the distribution of gas velocity in the furnace cavity, there was almost no air flow distribution in the conical section at the bottom of the furnace cavity, indicating that gas–solid heat transfer did not occur in this area. Therefore, the particles in this area were ignored in order to further reduce the number of particles and improve the calculation efficiency.

The final computational domain is shown in Figure 4a. The computational domain was meshed using tetrahedral cells. Due to the dense packing of particles, the mesh size could be even lower than 3 times the maximum particle diameter without compromising the grid independence of the particle volume fraction calculation. Therefore, the minimum mesh size was set to be 1.5 times the maximum particle diameter. The edge vent cowl tuyere and center vent cowl tuyere were set as velocity inlets. The wall above the center vent cowl was set as the symmetrical surface. The outlet plane of the distribution pipe was set to the pressure outlet, and the rest of the wall was set to wall, as shown in Figure 4b.

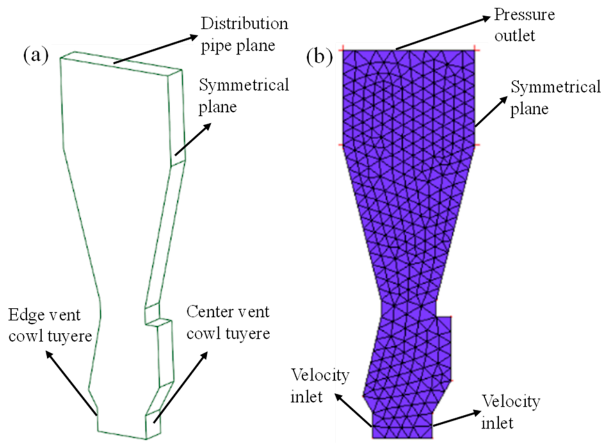

Figure 4. Computational domain and grid division. (**a**) Computational domain; (**b**) grid division.

3.3. Simulation Process

(1) Set a virtual buffer bin (not drawn) above the computational domain, with its bottom connected to the top of the computational domain. Calculate the accumulation process of constant mass particles in the buffer bin using the discrete element method. This is because when the fixed-bed heat transfer model is used, the particle size composition and the mass fraction of each particle size section should be consistent. If the particles are generated and accumulated directly in the calculation domain, the characteristics of a wide particle size distribution and the random generation of particles will cause differences in the mass and composition of particles contained in different Venturi furnace types, thereby affecting the gas–solid heat transfer.

(2) Discharge the particles from the buffer bin into the computational domain. According to the material distribution characteristics in the vertical cooling furnace [25], the segregation of particles in the furnace is the most severe in the initial stage of discharge. As the discharge progresses, the distribution segregation of materials is alleviated. In order to shorten the discharge time and make the particle distribution in Venturi furnaces with different structures relatively consistent, the entry mode of particles was changed so that the particles entered directly from the top of the calculation domain.

(3) Complete the accumulation of particles within the computational domain. Then, set the particle velocity to 0 m/s and delete the buffer bin. Subsequently, introduce the cooling gas from the edge and center vent cowl for the gas–solid heat transfer coupling calculation. After 2 s of heat exchange, stop the calculation and perform data processing.

According to the operation data of the Meishan Steel vertical cooling furnace, the entry temperatures of the sinter and the cooling gas were set to 773 K and 393 K, respectively. The qualitative temperature of both was the average of the temperature in and out of the vertical cooling furnace, and the qualitative temperatures of the sinter and the cooling gas were calculated to be 613 K and 483 K, respectively. The physical property parameters at the qualitative temperature were obtained by introducing the physical property parameter calculation formulas in Refs. [26–28]. See Table 4 for details.

Table 4. Simulation parameter settings.

Scaling Factor	Specific Heat Capacity (J/kg·K)	Thermal Conductivity (W/m·K)	Density (kg·m^{-3})	Dynamic Viscosity (kg/m·s)	Inlet Temperature (K)	Particle Mass (kg)	Superficial Velocity (m·s^{-1})
Cooling gas	1034.04	0.0382	0.726	2.64×10^{-5}	393	–	3.203
Sinter	817.36	8	2600	–	773	2400	–

4. Results and Discussion

4.1. Orthogonal Experimental Design

An orthogonal experiment is an efficient experimental method that uses an orthogonal table to arrange and analyze multi-factor experiments scientifically and to find the optimal level combination. It has the advantages of a smaller number of experiments, a uniform distribution of data points, a simple method, and strong reliability of the conclusions. According to the results of the analysis in the previous section, the structure of Venturi furnaces involves four factors: the width w and length l of the vertical part, the contraction angle of the contraction part β, and the expansion angle of the expansion part α.

The smaller the vertical section width w, the faster the cooling gas and sinter velocities, which increases the gas–solid heat transfer coefficient but also causes an increase in the pressure drop of the cooling gas passing through the region. However, the more important impact is the increased risk of sinter sticking. Ref. [29] points out that for spherical particles, the diameter of the circular discharge port should not be less than 6~8 or 6~10 times the maximum particle size. At the same time, for the convenience of equipment installation, the width of the upper center vent cowl should not be too small. The final value range of w was determined to be 1.0~1.2 m, which means the values were 1.0 m, 1.1 m, and 1.2 m.

The longer the length l of the vertical section, the longer the distance for gas to exchange heat with the sinter at a higher speed, which is beneficial for increasing the heat exchange capacity between gases and solids in the furnace but also leads to an increase in the pressure drop of gas passing through the material layer. The thickness of the material layer of the existing circular cooler is usually 0.76 m. In view of this, the length l of the vertical part was set to 0.7 m, 0.5 m, and 0.3 m.

The contraction angle β of the contraction part was equivalent to the half–top angle of the silo structure. Compared with the gas velocity, this value had a greater influence on the integrity of the downward movement of the sinter. Ref. [30] points out that under the condition of certain material parameters, the key factor determining whether the flow in the silo presents a funnel flow or a mass flow is the half–top angle of the silo, and it gives the formula for calculating the maximum half–top angle required to maintain the mass flow. According to the physical parameters provided in Ref. [31], the maximum half–top angle obtained using the above formula is 16.5°. Based on this, appropriate adjustments were made to obtain the values for β of 18°, 16°, and 14°.

The expansion angle α of the expansion part was equivalent to the residual angle of the blast furnace shaft. If α is too small, the effect of increasing the width of the furnace cavity will not be significant, while too great a value will increase the width of the furnace cavity too violently, resulting in the loose accumulation of particles on the side wall, thus increasing its voidage. Therefore, the expansion angle α was set to 13°, 15°, and 17°.

Based on the above parameters and their values, the L9 (3^4) orthogonal table was selected to arrange the orthogonal experimental plan, as shown in Table 5.

Table 5. Experimental factors and levels.

Levels	Factors			
	w/m	l/m	β/°	α/°
1	1.0	0.3	14	13
2	1.1	0.5	16	15
3	1.2	0.7	18	17

4.2. Evaluation Index

(1) Sensible heat recovery of the sinter

Firstly, the following equation was used to calculate the sensible heat recovery of the sinter during the heat exchange time:

$$Q_s = \sum_{i=1}^{N} c_i m_i (T_i^1 - T_i^0) \quad (1)$$

where Q_s is the heat recovered from the sinter, J; T_i^1 is the temperature of particle i after heat exchange, K; T_i^0 is the initial temperature of particle i, K; and N is the total number of particles in the furnace cavity.

In different experimental schemes, except for the difference in the structure of the Venturi furnace, which led to different sinter-stacking effects, all other factors were the same. Therefore, the difference in the sensible heat recovery of sinter was caused by different furnace structures. The more sensible the heat recovery of sinter, the more significant the improvement effect of the furnace structure on the gas–solid heat transfer effect.

(2) Gas pressure drop

At present, the gas pressure drop in the Meishan Steel vertical cooling furnace is relatively small, and the cooling gas cannot pass through the material layer evenly. With an increase in the pressure drop, the power for the cooling gas to enter the material layer increases, which is beneficial for the cooling gas to enter the material layer that could not be penetrated originally. But an excessive pressure drop will increase the costs and reduce the economy. Therefore, while considering the improvement in the gas–solid heat transfer efficiency, it is necessary to take into account the increase in the cooling gas pressure drop.

(3) Mass flow index (*MFI*) [32]

Due to the inability of the fixed-bed model to reflect the downward movement of the sinter in the furnace, the *MFI* was introduced to quantitatively study the flow characteristics of the sinter.

4.3. Experimental Results and Analysis

The results of the orthogonal experiment (schemes 1~9) are shown in Table 6. A range analysis was utilized to analyze the experimental results. Among the two main indicators examined, the higher the sensible heat recovery, the better. And the overall pressure drop should be appropriately small. The range analysis of the experimental results is shown in Table 7.

Table 6. Orthogonal experimental results.

Scheme	Factors				Results	
	w (m)	l (m)	β (°)	α (°)	Sensible Heat Recovery (J)	Pressure Drop (Pa)
1	1 (1.0)	1 (0.3)	1 (14)	1 (13)	505,706	8530
2	1	2 (0.5)	2 (16)	2 (15)	504,251	8164
3	1	3 (0.7)	3 (18)	3 (17)	504,318	8232
4	2 (1.1)	1	2	3	501,501	6663
5	2	2	3	1	503,068	7046
6	2	3	1	2	503,463	7934
7	3 (1.2)	1	3	2	499,240	6427
8	3	2	1	3	500,886	6996
9	3	3	2	1	501,029	7107

Table 7. Analysis of experimental results.

Factors		w (m)	l (m)	β (°)	α (°)
Sensible heat recovery (J)	K1	1,514,275	1,506,447	1,510,055	1,509,803
	K2	1,508,032	1,508,205	1,506,781	1,506,954
	K3	1,501,155	1,508,810	1,506,626	1,506,705
	k1	504,758.33	502,149	503,351.67	503,267.67
	k2	502,677.33	502,735	502,260.33	502,318
	k3	500,385	502,936.67	502,208.67	502,235
	R	4373.33	787.67	1143	1032.67
	Superior level	1	3	1	1
	Order of factors	$w > \beta > \alpha > l$			
Pressure drop (Pa)	K1	24,926	21,620	23,460	22,683
	K2	21,643	22,206	21,934	22,525
	K3	20,530	23,273	21,705	21,891
	k1	8308.67	7206.67	7820	7561
	k2	7214.33	7402	7311.33	7508.33
	k3	6843.33	7757.67	7235	7297
	R	1465.34	551	585	264
	Superior level	3	1	3	3
	Order of factors	$w > \beta > l > \alpha$			

According to the results of the range analysis, the influence order of the Venturi furnace structure parameters on the sensible heat recovery and the gas pressure drop of the sinter was different. For the sensible heat recovery, the width w of the vertical part had the greatest influence, followed by the contraction angle β and the expansion angle α, and their effects were similar. The length l of the vertical part had the least influence; for the pressure drop, the structural parameter with the greatest influence was still w. The next were β and l, and the effects of the two were similar. The influence of α was the smallest.

The trend in the sensible heat recovery and pressure drop was consistent, that is, the higher the sensible heat recovery, the greater the gas pressure drop, but there was a difference in the magnitude of the change between the two. The influence of individual structural parameters is shown in Figure 5. As shown in Figure 5a, when the vertical section width w was reduced, the sensible heat recovery increased approximately uniformly, while the pressure drop first increased slightly and then increased significantly. Therefore, the value of w can be set to 1.1 m to achieve a higher sensible heat recovery while avoiding excessive increases in the pressure drop. The contraction angle β was the second most important parameter affecting the sensible heat recovery and pressure drop, as shown in Figure 5b. When β decreased, both the sensible heat recovery and the pressure drop first increased slightly and then increased significantly. Therefore, the value of β can be set to 16°. The expansion angle α had a greater impact on the sensible heat recovery than on the pressure drop. As shown in Figure 5c, when α was reduced to 13°, the sensible heat recovery increased significantly. Therefore, the value of α can be set to 13°. The influence of the vertical section length l on the pressure drop exceeded that on the sensible heat recovery. As shown in Figure 5d, when l exceeded 0.5 m, the increase in the pressure drop became larger, and the increase in the sensible heat recovery became smaller. Therefore, the value of l was set to 0.5 m. In summary, the appropriate combination of structural parameters for the Venturi furnace is w = 1.1 m, β = 16°, α = 13°, and l = 0.5 m.

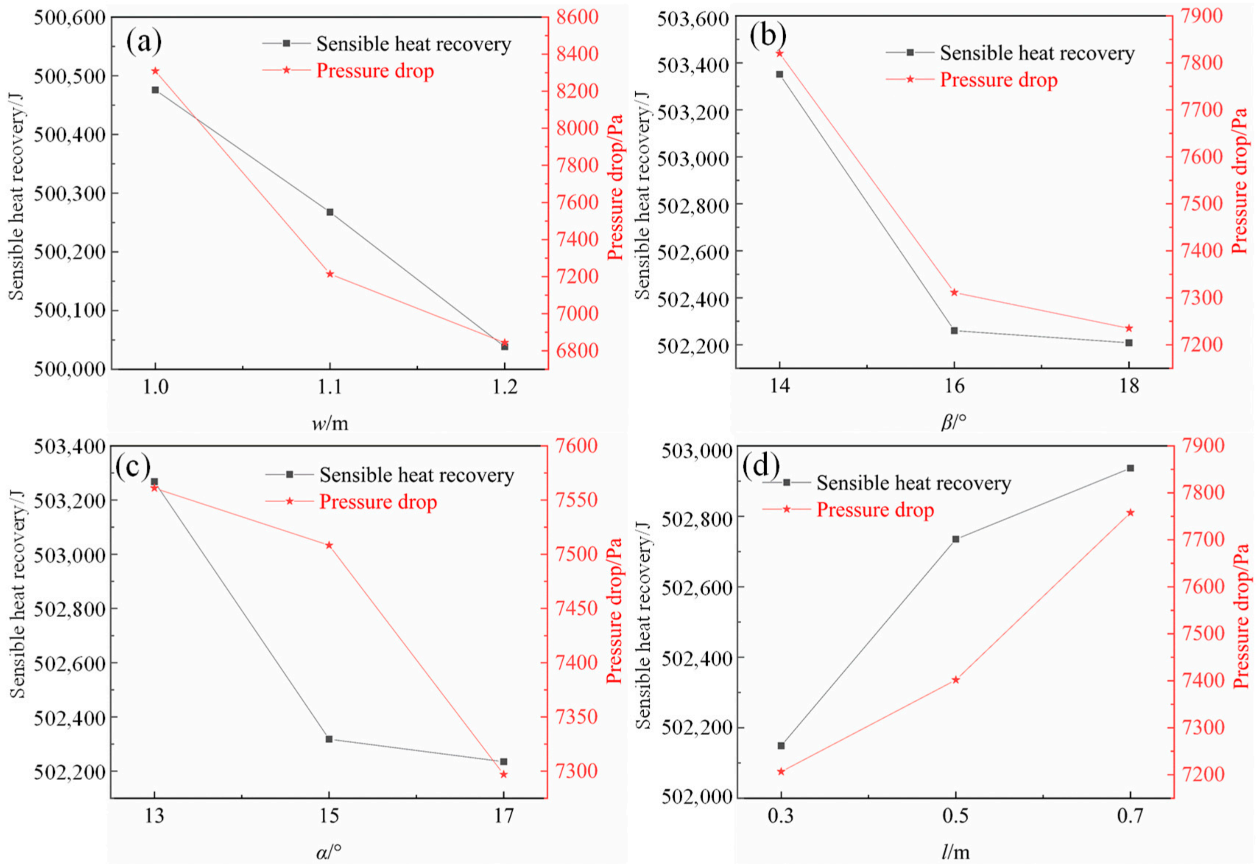

Figure 5. Influence of structural parameters. (**a**) w; (**b**) β; (**c**) α; (**d**) l.

The flow characteristics of the sinter in the obtained suitable Venturi furnace were studied. To improve the calculation efficiency, the discharge rate of the sinter was appropriately increased. The results are shown in Figure 6. It can be seen that after 90 s of discharge, the flow pattern of the sinter did not change much from that at 80 s. When the discharge of the material was continued for 100 s, the flow pattern of the sinter was still similar to that at 90 s. Therefore, it is believed that the downward movement of the sinter after 90 s of discharge reached a stable state. From Figure 6a, it can be seen that in the vertical section of the Venturi furnace obtained from the orthogonal experiments, the downward movement of particles in the sidewall area was suppressed, and the minimum *MFI* of particles was only 0.43. This is because the friction force on the particles in the central area of the vertical section was less than that in the sidewall area, making the downward movement of the particles in the central area smoother. After the Venturi structure was used, the width of the cavity for the downward movement of the material became narrow, causing particles in the sidewall area to be squeezed by particles in the central area and making it difficult for them to flow into the mainstream area, resulting in particle accumulation. Therefore, an attempt was made to install a baffle in the central area of the vertical section to increase the friction of the particles in the central area and balance the downward movement of the particles, as shown in Figure 6b. At this point, the downward distances of the particles in the sidewall area and central areas were basically the same. The minimum *MFI* of the particles in the vertical section was calculated to be 0.71, indicating that the fluidity of the sinter was significantly improved.

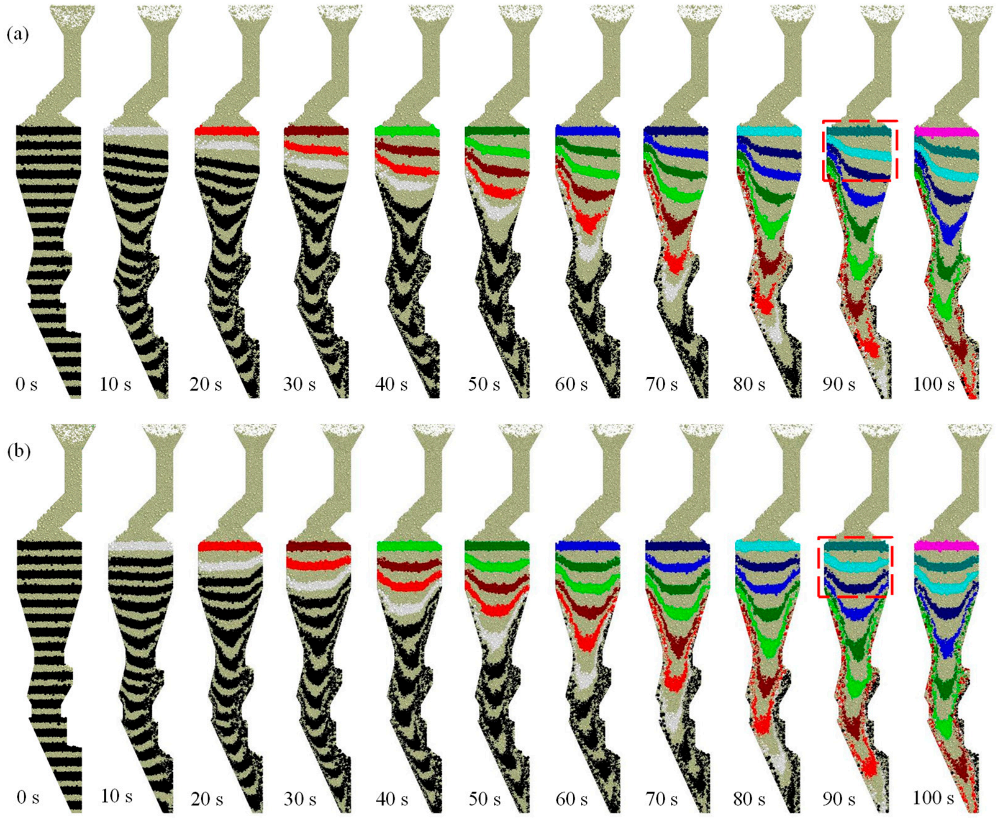

Figure 6. Comparison of material flow patterns in steady state. (**a**) Initial Venturi furnace type; (**b**) improved Venturi furnace type.

Under the same heat exchange conditions, the sensible heat recovery of the existing furnace type was compared with that of the improved Venturi furnace type, as shown in Figure 7. It can be seen that the improved Venturi furnace type could recover 504,864 J and reduce the pressure drop to 7053 Pa during the heat transfer time, both of which are higher than the existing furnace type's 493,976 J and 4088 Pa. Compared with the results of the orthogonal experiment, the sensible heat recovery was second only to scheme 1 in Table 6, but the pressure drop was lower than that of scheme 1. This is because the influence of l on the pressure drop of the gas was greater than that on the sensible heat recovery. The above results show that the improved Venturi furnace was effective in improving the gas–solid heat transfer and controlling the increase in the gas pressure drop.

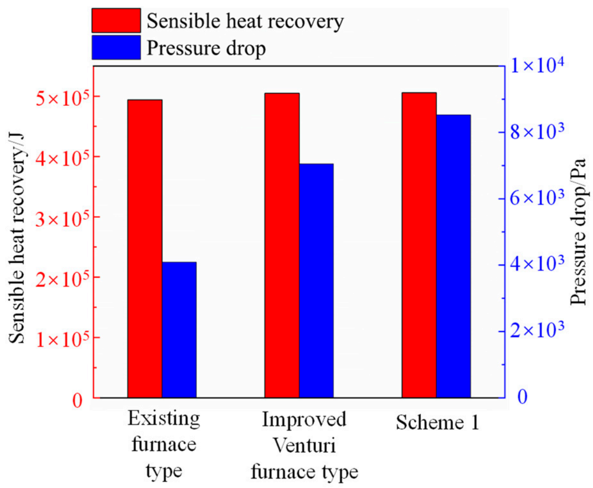

Figure 7. Comparison of sensible heat recovery and pressure drop among different schemes.

5. Conclusions

(1) A scaling factor was introduced to scale the physical model; only the upper limit of particle size was reduced, and the rest of the particle size and mass fraction remained unchanged. The scaling factor for the physical model was the same as the upper limit of granularity. Based on the results of a comparison of the particle quantity, porosity, and gas flow velocity distribution, the scaling factor was determined to be 0.7 to balance the simulation accuracy and computational cost.

(2) From the perspective of preventing material jamming, improving material flow integrity, facilitating installation, and reducing cooling gas pressure drop, the selection range of the structural parameters of a Meishan Steel Venturi shaft cooling furnace was determined.

(3) The results of the orthogonal experiments were as follows: For the sensible heat recovery, the width w of the vertical part had the greatest influence, followed by the contraction angle β and the expansion angle α, and their effects were similar. The length l of the vertical part had the least influence. For the pressure drop, the structural parameter with the greatest influence was still w. The next were β and l, and the effects of the two were also similar. The influence of α was the smallest.

(4) The higher the sensible heat recovery, the greater the gas pressure drop, but there was a difference in the trend of the two with the change in structural parameters. From the perspective of balancing the sensible heat recovery and the gas pressure drop, the appropriate structure parameters for the Venturi furnace were as follows: $w = 1.1$ m, $\beta = 16^\circ$, $\alpha = 13^\circ$, and $l = 0.5$ m.

(5) The fluidity of the material in the Venturi furnace with the above parameter combination was verified, and it was found that the *MFI* of the particles in the vertical section decreased to 0.43. After the wall friction experienced by the particles in the central area of the vertical section was increased, the *MFI* increased to 0.7, indicating that the integrity of the sinter flow in this furnace type can also be guaranteed.

(6) The results can provide theoretical guidance for the improvement of Meishan Steel vertical cooling furnaces. Of course, for the sake of comparison, this study maintained the existing operating parameters of Meishan Steel vertical cooling furnaces. Further research can be conducted on the operating parameters corresponding to the Venturi furnace type.

Author Contributions: Conceptualization, H.L.; data curation, T.Q.; funding acquisition, H.L.; investigation, H.L.; methodology, T.Q.; project administration, H.L.; resources, H.L.; software, T.Q.; supervision, Y.Z.; writing—original draft preparation, T.Q.; writing—review and editing, H.L. All authors have read and agreed to the published version of the manuscript.

Funding: This research was funded by the National Key R&D Program of China (grant number 2022YFE0208100) and the Fundamental Research Funds for the Central Universities (grant number N2225022), and the APC was funded by 2022YFE0208100.

Institutional Review Board Statement: Not applicable.

Informed Consent Statement: Not applicable.

Data Availability Statement: The data are contained within the article.

Acknowledgments: The authors sincerely acknowledge the anonymous reviewers for their insights and comments, which further improved the quality of the manuscript.

Conflicts of Interest: The authors declare no conflict of interest.

References

1. Tian, F.Y.; Huang, L.F.; Fan, L.W.; Qian, H.L.; Yu, Z.T. Wall effects on the pressure drop in packed beds of irregularly shaped sintered ore particles. *Powder Technol.* **2016**, *301*, 1284–1293. [CrossRef]
2. Li, J.G.; Li, J.; Wang, L.; Wang, Z.C. Comparative analysis of energy efficiency and investment of sintering waste heat power generation and SHRT process. *Sinter. Pelletiz.* **2023**, *48*, 15–23. (In Chinese)

3. Sun, K.; Tseng, C.T.; Wong, D.S.H.; Shieh, S.S.; Jang, S.S.; Kang, J.L.; Hsieh, W.D. Model predictive control for improving waste heat recovery in coke dry quenching processes. *Energy* **2015**, *80*, 275–283. [CrossRef]
4. Zheng, Y.; Dong, H.; Cai, J.J.; Feng, J.S.; Zhao, L.; Liu, J.Y.; Zhang, S. Experimental investigation of volumetric heat transfer coefficient in vertical moving–bed for sinter waste heat recovery. *Appl. Therm. Eng.* **2019**, *151*, 335–343. [CrossRef]
5. Xu, C.Y.; Liu, Z.C.; Wang, S.C.; Liu, W. Numerical simulation and optimization of waste heat recovery in a sinter vertical tank. *Energies* **2019**, *12*, 385. [CrossRef]
6. Feng, J.S.; Zhao, L.; Zhang, S.; Dong, H. Exergy analysis and parameter optimization of sinter cooling process in vertical moving bed for waste heat recovery. *Appl. Therm. Eng.* **2020**, *175*, 115370. [CrossRef]
7. Feng, J.S.; Dong, H.; Gao, J.Y.; Li, H.Z.; Liu, J.Y. Numerical investigation of gas–solid heat transfer process in vertical tank for sinter waste heat recovery. *Appl. Therm. Eng.* **2016**, *107*, 135–143. [CrossRef]
8. Fu, J.P.; Cai, J.J. Numerical investigation and optimisation of heat transfer performance in a vertical sinter cooling packed bed using Taguchi and ANOVA methods. *Iron Steel Res. Int.* **2020**, *27*, 898–912. [CrossRef]
9. Chen, S.B.; Sai, Q.Y.; Ding, H.G.; Peng, Y. Numerical simulation of gas flow and heat transfer in a vertical tank for sintering waste heat recovery. *J. Eng. Therm. Energy Power* **2018**, *33*, 87–94. (In Chinese)
10. Zhang, S.; Zhao, L.; Feng, J.S.; Luo, X.F.; Dong, H. Thermal analysis of sinter vertical cooler based on waste heat recovery. *Appl. Therm. Eng.* **2019**, *157*, 113708. [CrossRef]
11. Xu, T.J.; Zhang, S.; Gao, J.Y.; Feng, J.S.; Dong, H. Determination method of thermal parameters of vertical tank for sinter waste heat recovery and its application. *Iron Steel* **2018**, *53*, 107–112. (In Chinese)
12. Bi, C.G.; Sun, J.J. Application of process to recycle sensible heat of sinter using vertical cooling furnace in Meisteel. *Sinter. Pelletiz.* **2018**, *43*, 69–72. (In Chinese)
13. Qi, T.F.; Li, H.F.; Sun, J.J.; Chen, G.J.; Zhang, Y.J. Simulation of gas-solid flow in sinter vertical cooling furnace. *Iron Steel Res. Int.* **2023**, *30*, 2133–2142. [CrossRef]
14. Qi, T.F.; Li, H.F.; Zhang, Y.J.; Shao, L. Influence of variable–diameter structure on gas–solid heat transfer in vertical shaft cooler. *Metals* **2022**, *12*, 1187. [CrossRef]
15. Li, H.F.; Qi, T.F.; Zhang, Y.J. Effect of furnace structure on burden distribution and gas flow in sinter vertical cooling furnace. *Appl. Sci.* **2023**, *13*, 11268. [CrossRef]
16. Chaudhuri, B.; Muzzio, F.J.; Tomassone, M.S. Modeling of heat transfer in granular flow in rotating vessels. *Chem. Eng. Sci.* **2006**, *61*, 6348–6360. [CrossRef]
17. Dong, Z.S.; Xue, Q.G.; Zuo, H.B.; She, X.F.; Li, J.; Wang, J.S. Gas–solid flow and shaft injected gas penetration in an oxygen blast furnace analyzed using a three–dimensional DEM–CFD coupling mathematical model. *ISIJ Int.* **2016**, *56*, 1588–1597. [CrossRef]
18. Zhang, S.; Zhao, L.; Feng, J.S.; Dong, H. Numerical investigation of the air–particles heat transfer characteristics of moving bed-effect of particle size distribution. *Int. J. Heat Mass Transf.* **2022**, *182*, 122036. [CrossRef]
19. Wei, G.C.; Zhang, H.; An, X.Z.; Xiong, B.; Jiang, S.Q. CFD–DEM study on heat transfer characteristics and microstructure of the blast furnace raceway with ellipsoidal particles. *Powder Technol.* **2019**, *346*, 350–362. [CrossRef]
20. Qiu, L.; Sang, D.W.; Li, Y.L.; Feng, Y.H.; Zhang, X.X. Numerical simulation of gas–solid heat transfer characteristics of porous structure composed of high–temperature particles in moving bed. *Appl. Therm. Eng.* **2020**, *181*, 115925. [CrossRef]
21. Feng, J.S.; Dong, H.; Liu, J.Y.; Liang, K.; Gao, J.Y. Experimental study of gas flow characteristics in vertical tank for sinter waste heat recovery. *Appl. Therm. Eng.* **2015**, *91*, 73–79. [CrossRef]
22. Zhang, X.K.; Xu, J.; Sun, J.J.; Zhang, Y.J.; Zhang, Z.H.; Ge, W. Segregation behavior of sinter in vertically arranged cooler with high performance GPU simulation. *Chin. J. Mech.* **2019**, *51*, 64–73. (In Chinese)
23. Zhu, H.P.; Yu, A.B. The effect of wall and rolling resistance on the couple stress of granular materials in vertical flow. *Phys. A* **2003**, *325*, 347–360. [CrossRef]
24. Dong, Z.S.; Wang, J.S.; Zuo, H.B.; She, X.F.; Xue, Q.G. Analysis of gas–solid flow and shaft-injected gas distribution in an oxygen blast furnace using a discrete element method and computational fluid dynamics coupled model. *Particuology* **2017**, *32*, 63–72. [CrossRef]
25. Qi, T.F.; Huang, J.; Sun, J.J.; Zhang, Y.J. DEM simulation of sinter distribution in vertical cooling furnace. *China Metall.* **2022**, *32*, 20–26. (In Chinese)
26. Pan, L.S.; Wei, X.L.; Peng, Y.; Ma, Y.J.; Li, B. Theoretical study on the cooling procedure for vertical flow sinters. *Appl. Therm. Eng.* **2017**, *127*, 592–601. [CrossRef]
27. Tian, F.Y.; Huang, L.F.; Fan, L.W.; Weng, Y.K.; Ying, X.Y.; Yu, Z.T.; Cen, K.F. A comprehensive characterization on the structural thermophysical properties of sintered ore particles toward waste heat recovery applications. *Appl. Therm. Eng.* **2015**, *90*, 1007–1014. [CrossRef]
28. Zhang, S.; Zhao, L.; Feng, J.S.; Luo, X.F.; Dong, H. Parameter optimization of gas–solid heat transfer process in sinter packed bed based on further exergy analysis. *Chem. Eng. Res. Des.* **2019**, *146*, 499–508. [CrossRef]
29. Jenike, A.W. Storage and flow of solids, bulletin No. 123. *Bull. Univ. Utah* **1964**, *53*, 229–236.
30. Tan, Y.Q.; Xiao, X.W.; Zheng, J.H.; Jiang, S.Q.; Gao, W. Effect of outlet diameter of cone–in–cone insert on silo flow pattern. *Trans. CSAE* **2016**, *32*, 82–87. (In Chinese)

31. Chen, T.; Zhang, S.; Zhao, L.; Feng, J.S.; Dong, H. Determination and calibration of DEM parameters for sinter particles. *Iron Steel Res.* **2023**, *35*, 24–32. (In Chinese)
32. Liu, Y.L.; Liu, S.Q.; Zhao, X.Q.; Liu, C.; Zhang, Z. Flow characteristics of granule discharged from eccentric wedge–shaped feed hopper. *CIESC J.* **2018**, *69*, 1469–1475. (In Chinese)